Applied Catalysis B: Environmental 238 (2018) 177–183

Contents lists available at ScienceDirect

Applied Catalysis B: Environmental

journal homepage: www.elsevier.com/locate/apcatb

Black hollow TiO_2 nanocubes: Advanced nanoarchitectures for efficient visible light photocatalytic applications

Abolfazl Ziarati[a], Alireza Badiei[a,**], Rafael Luque[b,c,*]

[a] School of Chemistry, College of Science, University of Tehran, Tehran, Iran
[b] Departamento de Quimica Organica, Universidad de Cordoba, Campus de Rabanales, Edificio Marie Curie, E-14014 Cordoba, Spain
[c] Peoples Friendship University of Russia (RUDN University), 6 Miklukho-Maklaya str., 117198, Moscow, Russia

ARTICLE INFO

Keywords:
Hollow structures
Visible light photocatalysis
Hydrogenated TiO_2
Nanoarchitecture
Benzimidazole synthesis

ABSTRACT

Black hollow nanocubic TiO_2 (BHC-TiO_2) architectures have been synthesized via multi-step approach comprising co-precipitation to prepare hematite nanocubes; titania covering of hematite towards Fe_2O_3/TiO_2 core/shell nanocubes and hydrothermal hematite etching process to yield hollow cubic TiO_2 structures with Ti^{3+} species after high temperature hydrogen treatment. The resultant BHC-TiO_2 nanoarchitectures exhibited excelling photocatalytic performance under visible light in the preparation of benzimidazole derivatives. This superior activity can be attributed to the design of BHC-TiO_2 with high surface area (~206 m^2g^{-1}), ultrathin shell (~50 nm), hydrogenated visible active structure and void nanoreactor-like space in the cubic structure.

1. Introduction

Organic chemicals are necessary for the preparation of a great number of end products and compounds including pesticides, pharmaceuticals, and food additives which are an integral part of everyday life. Conventional industrial methods for many essential organic chemicals typically involve harsh operating conditions such as high pressures and temperatures. The development of environmentally benign synthetic processes which rely on renewable energy sources to drive chemical reactions under much milder reaction conditions is highly desirable [1]. Solar energy, is an ideal energy source to overcome future environmental challenges in energy demanding processes/technologies [2]. Considering that, in one hour, the sun delivers sufficient energy to all human actions on the planet for an entire year, the harvesting of sunlight by artificial photocatalysts and its utilization as source of energy can be highly attractive, particularly to promote organic reactions, [3,4].

TiO_2 received most attention in recent years as photocatalyst due to its chemical and biological inertness, cost effectiveness and the robust oxidizing power of its photogenerated holes [5]. However, one of the major barriers of using pure TiO_2 is that only ultraviolet light photons can displace the valence band electrons of TiO_2 due to its high bandgap energy (3.2 eV), making use only of ca. 5% of the solar radiation. Furthermore, the high recombination rate (about 90%) of photon induced electron-hole pairs reduces the photocatalytic productivity of TiO_2 [6].

Previous reports have indicated that physico-chemical properties of TiO_2 including surface area, particle size and morphologies can strongly influence photocatalytic efficiencies [7–9]. Among various TiO_2 morphologies, hollow structures have received increasing attention because of their unusual properties which include high specific surface areas, enhanced light absorption, and high electron-hole separation [10,11]. Hollow structures do not only enhance the effectiveness of light utilization by multiple reflections of light within the interior cavity, but can also act as *nanoreactor-like* (confinement effects) and allow an effective diffusion of solvents, reactants and products *in-and-out* of the inner vacancies through the porous shells [12]. Owing to these remarkable structural properties, different types of TiO_2 hollow structures have been recently employed in various photocatalytic processes [13–15].

Yin et al. have prepared mesoporous TiO_2 hollow shells through a hard template route with good photocatalytic activity for the decomposition of organic dye molecules [16]. Yang et al. have synthesized hollow TiO_2 hierarchical boxes with suitable anatase and rutile ratios with high light conversion abilities [17]. All prepared structures displayed enhanced light harvesting properties as compared to commercial TiO_2. However, to improve these advantages, herein we propose an alternative type of hollow structure featuring a cubic nanoarchitecture and hydrogenated surface, since as mentioned above, TiO_2-related applications are critically hindered by ineffective harvesting of visible

* Corresponding author at: Departamento de Quimica Organica, Universidad de Cordoba, Campus de Rabanales, Edificio Marie Curie, E-14014 Cordoba, Spain.
** Corresponding author at: School of Chemistry, College of Science, University of Tehran, Tehran, Iran.
E-mail addresses: abadiei@khayam.ut.ac.ir (A. Badiei), rafael.luque@uco.es (R. Luque).

https://doi.org/10.1016/j.apcatb.2018.07.020
Received 16 April 2018; Received in revised form 5 July 2018; Accepted 8 July 2018
Available online 10 July 2018
0926-3373/ © 2018 Elsevier B.V. All rights reserved.

light.

Reduced TiO_2 containing Ti^{3+} species have been considered as additionally advantageous to increase visible light photoactivities [18–23]. The improved photocatalytic efficiencies of hydrogenated TiO_2 have been ascribed to the role of surface Ti−H bonds in modifying optical absorption and an effective photo generated electron–hole separation [24,25]. In other cases, greater photo-activities of reduced TiO_2 nanocrystals have been ascribed to the presence of oxygen vacancies [26]. A concentration of Ti^{3+} in the surface of reduced TiO_2 has been proposed to be important in creating a facile transfer of an electron or hole [27].

Based on these premises, the design of TiO_2 nanomaterials with hollow cubic structure containing ultra-thin hydrogenated shells as smart nanoarchitecture for photocatalytic applications can lead to the next generation of advanced nanophotocatalytic materials. In continuation with research endeavours from our groups [28–33], herein we report a simple and efficient route to design hydrogenated hollow cubic TiO_2 nanoarchitectures (BHC-TiO_2) as efficient photocatalysts for benzimidazole derivatives preparation at room temperature under visible light irradiation.

2. Experimental

2.1. Preparation of cubic Fe_2O_3

Hematite nanocubes were prepared according to a previously reported method [34]. Briefly, 27.03 g $FeCl_3.6H_2O$ was added to 50 mL deionized water and stirred till a transparent solution was obtained. The solution was subsequently heated up to 75 °C and then 50 mL of 5.4 M NaOH solution was added dropwise to the above solution during a period of 5 min (further reacted for 10 min under stirring). The obtained gel was then transferred into a 100 mL Teflon-lined autoclave and the solution was kept at 100 °C for 56 h in a preheated oven. After the synthesis, the autoclave was cooled down to room temperature and the precipitate was separated by centrifugation, washed with water and ethanol (3 times) and dried overnight at 80 °C.

2.2. Preparation of Fe_2O_3/TiO_2 core/shell nanocubes

Fe_2O_3/TiO_2 core/shell nanocubes were prepared according to the reported versatile kinetically-controlled coating method [35]. *As prepared* Fe_2O_3 nanocubes (0.15 g) were dispersed in 100 mL absolute ethanol and mixed with 0.30 mL concentrated ammonia solution (28 wt.%) under ultrasonic irradiation for 15 min. 0.75 mL of TBOT was subsequently added dropwise (during 5 min) and the reaction was allowed to proceed for 24 h at 45 °C under continuous stirring. The resultant products were separated and collected, followed by washing with ethanol (3 times) and drying overnight at 80 °C.

2.3. Preparation of hollow TiO_2 nanocubes (HC-TiO_2)

Hollow cubic TiO_2 were prepared by mild acidic etching of the hematite core [36]. In a typical synthesis, 0.2 g of as prepared Fe_2O_3/TiO_2 core/shell nanocubes were mixed with 10 mL HCl solution (0.5 M). The stirred solution was sonicated for 10 min at room temperature and the obtained suspension was transferred into a Teflon-lined stainless steel autoclave (15 mL capacity) and aged at 100 °C for 24 h. The resulting mixture was subsequently centrifuged and washed several times with deionized water (until pH value was close to 7) and finally oven-dried at 80 °C for 12 h.

2.4. Preparation of hydrogenated hollow TiO_2 nanocubes

The resulting hollow TiO_2 nanocubes were calcined at 550 °C (the heating rate is 3 °C/min) for 3 h at 200 psi flow pressure under H_2/Ar (1:1) atmosphere. At the end of the heating period, the sample was cooled down to room temperature under H_2/Ar atmosphere. Sample was denoted as BHC-TiO_2.

2.5. Photocatalytic reaction experiments

Visible light photocatalytic reactions were conducted in parallel photoreaction cells (12 × 5 mL) made of Pyrex glass with continuous O_2 bubbling (10 psi flow pressure) and water recirculation to control the temperature (25 °C) during the experiments. A halogen lamp (Osram, 220 V and 500 W) was employed as visible light source.

UV light photocatalytic reactions were carried out at room temperature in a batch quartz reactor with the continuous O_2 bubbling (10 psi flow pressure). Artificial UV irradiation was provided by a 15 W (UV–C) mercury lamp (Philips, Holland) emitting around 254 nm, positioned in top of the batch quartz reactor.

For each experiment, 6 mg of catalyst was dispersed in the mixed solution of benzyl alcohols (3 mL) and *ortho*-phenylenediamine (1 mmol) under continuous O_2 bubbling. Prior to light irradiation, the mixtures were stirred for 1 h in the dark to achieve the adsorption–desorption equilibrium for benzyl alcohols and dissolved oxygen on the surface of photocatalyst. The photocatalytic reactions were carried out in 12 parallel reaction cells (aiming for identical conditions in all reactions) under magnetic stirring in presence of light for 7 h. At the end of reaction, about 1 mL of suspension was withdrawn and centrifuged to remove the remaining catalyst. The concentrations of benzimidazole were measured using GC (Varian CP 3800 instrument using silicon DC-200 or carbowax 20 M columns).

3. Results and discussion

3.1. Photocatalyst preparation and characterizations

Fig. 1 show a schematic illustration of the process and the corresponding FESEM, SEM-BSE and TEM images of the structures from each preparation step. As shown in Fig. 1a–d, the synthetic procedure includes the following main steps: a) co-precipitation preparation of Fe_2O_3 nanocubes as template, b) kinetically-controlled coating of Fe_2O_3 with TiO_2 to generate Fe_2O_3/TiO_2 core/shell nanocubes, c) HCl hydrothermal etching process to yield hollow cubic TiO_2, and d) hydrogen treatment to obtain BHC-TiO_2 nanoarchitectures.

Fig. 1(e–h) show FESEM images of BHC-TiO_2 for each step. Images clearly indicate that the cubic Fe_2O_3 particles are highly uniform structures with sizes of ca. 800 nm. Mono disperse core/shell structures of Fe_2O_3/TiO_2 cubes can be also visualized in Fig. 1f. After removing the core Fe_2O_3 templates by hydrochloric acid etching, the cubic TiO_2 structure is well maintained as demonstrated in Fig. 1g. The unique structures of the hollow cubic TiO_2 after hydrogen treatment are also illustrated in Fig. 1h, from which a number of nicely and homogeneously distributed BHC-TiO_2 nanocubes can be visualised. From the cracked BHC-TiO_2 structure (indicated by white arrows), the hollow cubic structure with ultrathin shell is evidently obvious. SEM-BSE micrographs relevant to each step are also depicted in Fig. 1(i–l). Fig. 1i and j showed the cubic Fe_2O_3 core and core/shell structure of Fe_2O_3/TiO_2 nanocubes with a solid hematite core and transparent titania shell, respectively. Fig. 1k and l showed the hollow cubic structure of TiO_2 shell before and after hydrogen treatment. Transparent ultrathin cubic structures confirmed the hollow cubic structures in both samples.

Fig. 1(m–p) displayed TEM images for each step of BHC-TiO_2 preparations. As shown in Fig. 1m, the cubic structure of Fe_2O_3 nanoparticles was evidenced. Fig. 1n shows the TEM image of core/shell Fe_2O_3/TiO_2 nanocubes that indicated a TiO_2 phase uniformly covering the surface of cubic Fe_2O_3. Fig. 1o showed a TEM image of the hollow cubic TiO_2 after template removing. As shown in Fig. 1p, the hollow cubic structure with ultrathin shell thickness (about 50 nm) is clearly visible.

HRTEM images of commercial TiO_2 (C-TiO_2) (Fig. 2a) and BHC-TiO_2

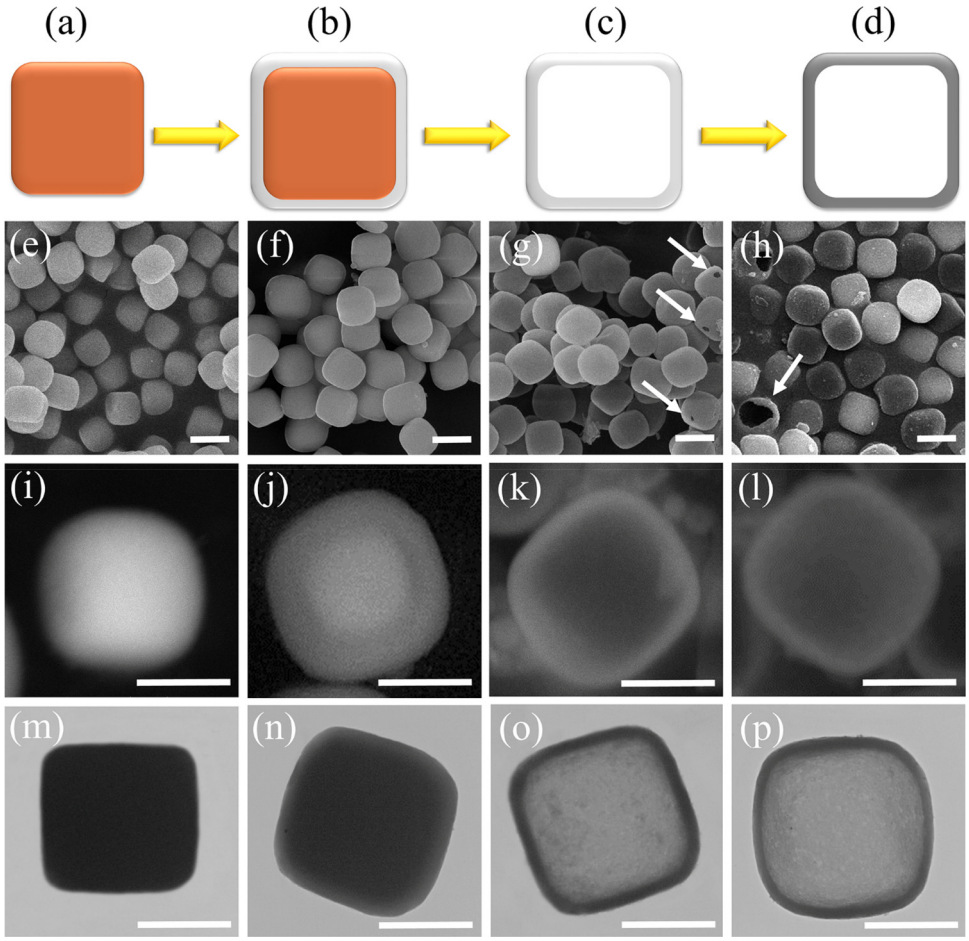

Fig. 1. Overall flowchart for fabrication of BHC-TiO_2 (a–d); corresponding FESEM (e–h), BSE-SEM (i–l) and TEM (m–p) images of the BHC-TiO_2 fabrication procedure. the white arrows indicate the cracked hollow cubic structures. The scale bars are 1 μm (e–h) and 500 nm (i–p).

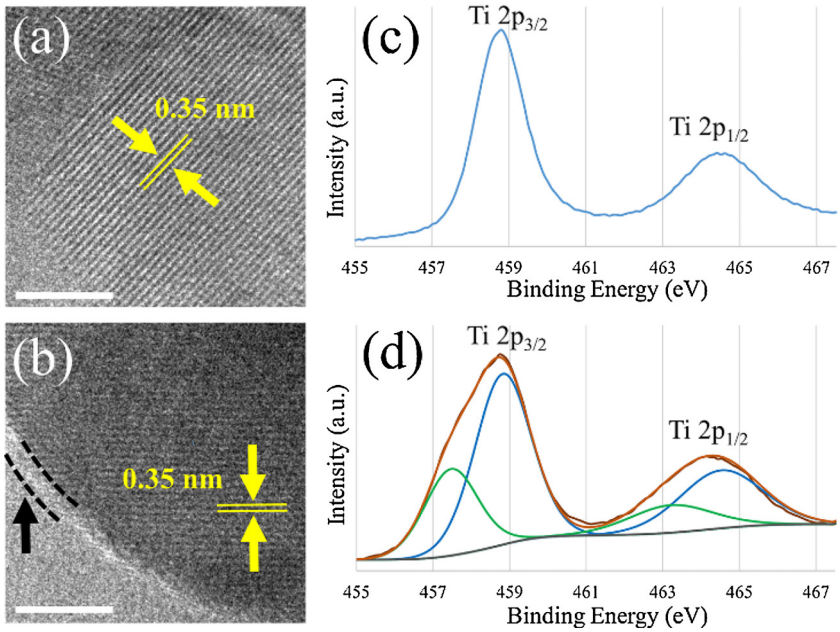

Fig. 2. HRTEM images of C-TiO_2 (a) and BHC-TiO_2 (b). XPS Ti 2p spectra of C-TiO_2 (c) and BHC-TiO_2 (d). Scale bars: 5 nm.

(Fig. 2b) structures show that both structures are highly crystalline, with a lattice spacing of 0.35 nm between (101) TiO_2 planes (yellow arrows). Furthermore, as indicated in Fig. 2b, a thin disordered surface layer encircling the crystalline structure could be clearly observed (white arrows). This can be attributed to the effect of hydrogen treatment and the generation of Ti^{3+} ions near the surface [37,38].

The chemical composition of BHC-TiO_2 was further studied by XPS analysis with respect to C-TiO_2 (Fig. 2(c, d)). XPS discloses the elements and associated chemical bonds in the top few atomic layers of the material, because the escape depth of electrons is a few nanometres. Two peaks of Ti $2p_{3/2}$ and Ti $2p_{1/2}$ can be observed in the high resolution Ti 2p XPS spectrum of C-TiO_2 and BHC-TiO_2 structures.

After deconvolution, Ti 2p peaks of BHC-TiO_2 comprise four main contributions at 457.6 eV, 458.8 eV, 463.3 eV and 464.6 eV. The peaks at 458.8 and 464.6 eV could be assigned to $2p_{3/2}$ and $2p_{1/2}$ core levels of Ti^{4+} [39], whereas the peaks at 457.6 and 463.3 eV are attributable to the $2p_{3/2}$ and $2p_{1/2}$ core levels of Ti^{3+} [40], respectively. These results support the existence of Ti^{3+} ions on the surface of BHC-TiO_2. The relative content of Ti^{3+} ions was roughly calculated to be ca. 35% by comparing XPS peak areas of Ti^{3+} vs Ti^{4+}.

The valence band position of BHC-TiO_2 was further studied by XPS analysis in comparison to C-TiO_2 (Fig. S1, see Supporting information). XPS spectra remained virtually identical for BHC-TiO_2 and C-TiO_2. The absence of any changes as a result of the hydrogenation process was also previously reported [41].

In order to investigate the elemental distribution in BHC-TiO_2 nanocubes, the elemental mapping of Ti and O were carried out by EDS area scanning as shown in Fig. S2. Mapping of Ti and O are well-defined with sharp contrast. In addition, the profile of Fe could not be observed, which indicates that the hematite core was completely removed during the etching process.

Raman spectra were measured to investigate the structural alterations on the surface of hollow cubic TiO_2 before and after hydrogen treatment, with C-TiO_2 also tested here as benchmark (Fig. 3). Well-resolved Raman peaks were observed around 145 cm^{-1} (B_{1g}), 395 cm^{-1} (B_{1g}), 515 cm^{-1} (E_g), and 640 cm^{-1} (E_g) in the spectra of all samples, indicating that anatase nanoparticles are predominant species. Interestingly, Raman spectra of BHC-TiO_2 indicated notable differences and two relevant features could be observed. Firstly, the two Eg modes of C-TiO_2 and HC-TiO_2 were found to be shifted to higher frequencies in BHC-TiO_2 due to decreasing of correlation length resulting from localized oxygen defective vacancies. Secondly, the peaks become weaker after hydrogen treatment. The presence of the oxygen vacancies lead to the change of atomic coordination numbers and bonding length of the Ti—O—Ti network in BHC-TiO_2. Therefore, the intensities of Raman peaks will decrease with an increase in the Ti^{3+}/Ti^{4+} molar ratio.These

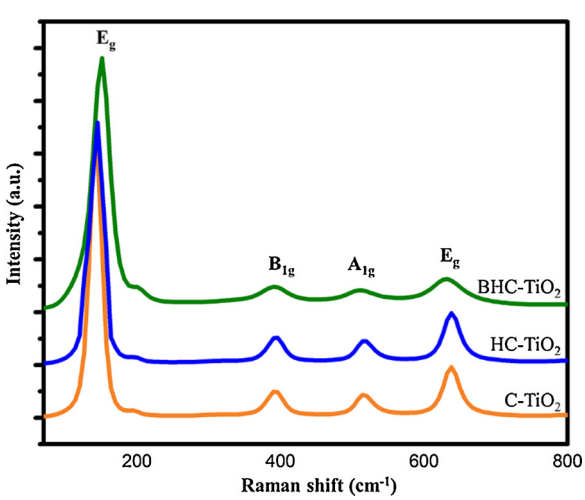

Fig. 3. Raman spectra of C-TiO_2, HC-TiO_2 and BHC-TiO_2.

weakened peaks after hydrogen treatment therefore support an increase in the number of oxygen vacancies in the lattice of BHC-TiO_2 structure due to the introduction of Ti^{3+}species into the lattice. These two features proved the increase of Ti^{3+} ions in the lattice structure of hollow cubic TiO_2 after hydrogenation [42,43].

Fig. S3 depicts XRD patterns of C-TiO_2 and BHC-TiO_2 architectures. The anatase phase of C-TiO_2 was found to be preserved upon hydrogenation. The sharp anatase (101) reflection of BHC-TiO_2 compared to that of C-TiO_2 can be attributed to the growth of crystallinity during the high temperature hydrogenation process. However, the diffraction reflections of BHC-TiO_2 give a slight shift towards a higher diffraction angle, suggesting the reduction of the interplanar distance of the crystalline phase. This result indicates that structural changes have occurred in titania during the hydrogenation process [44,45].

Photoluminescence (PL) spectra are useful to understand the behaviour of light-generated electrons and holes in photocatalysts since PL emission results from the recombination of electrons and holes. PL spectra of C-TiO_2, HC-TiO_2 and BHC-TiO_2 structures in the wavelength range of 350–700 nm with excitation at 320 nm are shown in Fig. S4. PL intensities for HC-TiO_2 slightly decrease as compared to C-TiO_2. This observation may be due to higher surface area and therefore a large concentration of sites in the surface of HC-TiO_2 for distribution and separation of electrons and holes from each other. Interestingly, PL intensities for BHC-TiO_2 were found to be weaker with respect to those of C-TiO_2 and HC-TiO_2 structures. This result pointed out that the recombination rate of photogenerated electrons and holes has been considerably inhibited in BHC-TiO_2 nanoarchitectures, because of the formation of oxygen vacancies during the hydrogenation step. Oxygen vacancies actually served as electron capture traps, and hence separated the charge carriers and significantly reducing the recombination.

UV–vis absorption spectra were measured to confirm the photoactivity of BHC-TiO_2 nanoarchitectures as presented in Fig. 4. No considerable response is observed in C-TiO_2 spectrum within the visible light range (400 and 700 nm). However, the spectrum of BHC-TiO_2 exhibits a strong absorption response in the visible region, most probably due to the presence of Ti^{3+} ions on the surface.

A new energy level may be created due to the presence of Ti^{3+} ions below the conduction band, resulting in the robust response in the visible region. The absorption of visible light illustrates that visible light can activate Ti^{3+} self-doped hollow cubic TiO_2 architecture, and more electrons and holes can be produced in photocatalytic reactions, providing a potentially to improved photoactivity. The calculated energy of the band gap of BHC-TiO_2 from the UV–vis spectrum is 2.41 eV (Fig. 4b).

To obtain insights into the porosity of BHC-TiO_2, BET surface areas and pore-size distributions using nitrogen adsorption and desorption isotherms were investigated. C-TiO_2 and HC-TiO_2 were also tested here as benchmark. As shown in Fig. 5, the BET surface area of BHC-TiO_2 is significant (206 $m^2 g^{-1}$), nearly five times larger to that of C-TiO_2 (41 $m^2 g^{-1}$) and ca. 15% higher than HC-TiO_2 (177 $m^2. g^{-1}$). BHC-TiO_2 isotherms also exhibited classic type IV curves according to the IUPAC classification, revealing a hysteresis loop at high relatively pressures associated with capillary condensation of gases within mesopores. The hysteresis loop is of type H2, consistent with pores with necks and wider bodies. This result demonstrates that porosity changes occurred rendering a large surface area BHC-TiO_2 material during the synthetic process.

3.2. Photocatalytic activity

The unique hydrogenated hollow cubic nanoarchitecture with high surface area, void inner space (potentially acting as "*nanoreactor*") as well as visible light absorption make BHC-TiO_2 an ideal candidate for photocatalytic applications. The photocatalytic performance of BHC-TiO_2 was tested in the synthesis of benzimidazole using benzyl alcohol and *ortho*-phenylenediamine as a model reaction. Fig. 6 shows that all

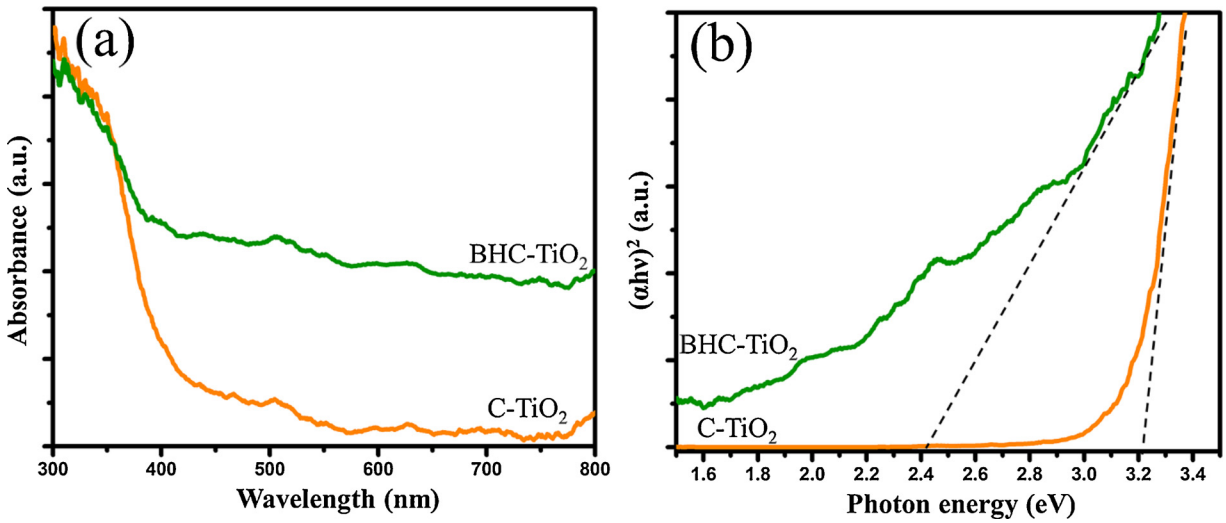

Fig. 4. UV–vis spectra (a) and plot of $(\alpha h\nu)^2$ vs. $h\nu$ (b) for C-TiO_2 and BHC-TiO_2.

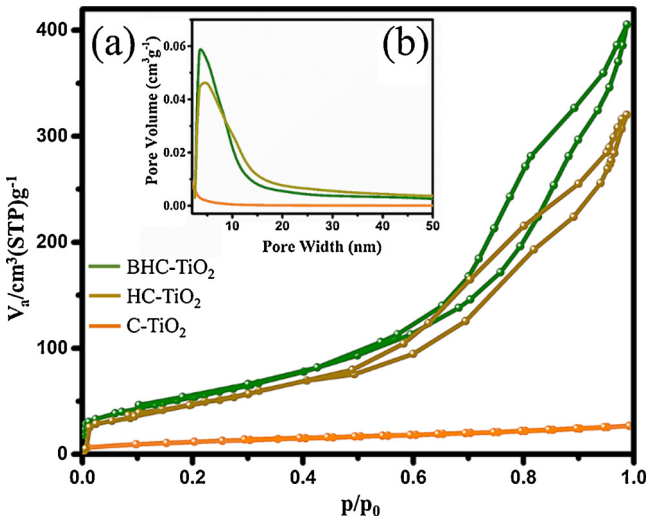

Fig. 5. Nitrogen adsorption-desorption isotherms of C-TiO_2, HC-TiO_2 and BHC-TiO_2.

Table 1
Visible light synthesis of benzimidazoles using BHC-TiO_2 nanocubes.[a]

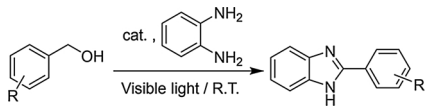

Entry	R	t [h]	Yield[b] (%)
1	H	7	86
2	4-Me	7	83
3	3-Me	7	79
4	4-OMe	7	82
5[c]	4-NO_2	7	81
6[c]	4-Cl	7	84
7[c]	2-Cl	7	77

[a] Reaction conditions: photocatalyst (6 mg), alcohol (3 mL), diamine (1 mmol), O_2 bubbling (10 psi flow), 298 K.
[b] GC-yield.
[c] Alcohol (2 mmol), acetonitrile (3 mL).

synthesized TiO_2 samples possess some oxidation photoactivity in the selected test reaction under UV irradiation Interestingly, C-TiO_2 and HC-TiO_2 displayed a low photocatalytic activity towards benzimidazole production under visible light irradiation. BHC-TiO_2 prepared by

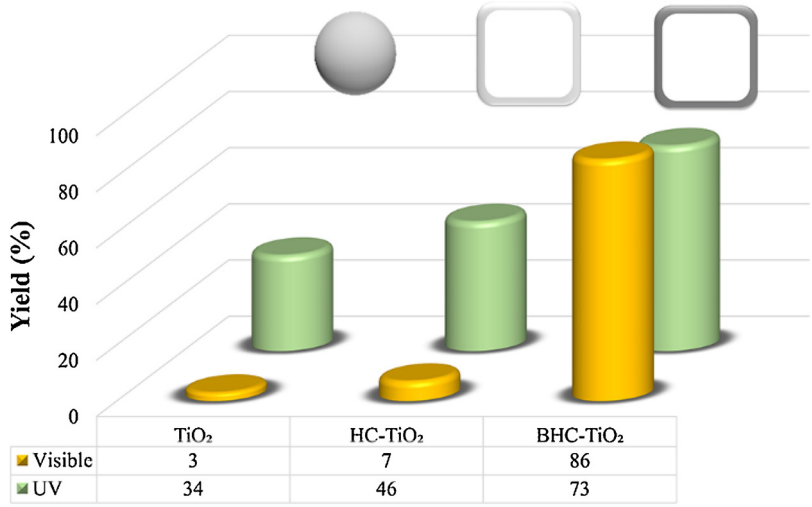

Fig. 6. Comparison photocatalytic activity of C-TiO_2, HC-TiO_2 and BHC-TiO_2 structures in the synthesis of benzimidazole under UV and visible conditions.

etching of hematite core and hydrogen treating of HC-TiO_2 comparably exhibited a remarkable photocatalytic activity (86% conversion), over a 28-fold increase to that observed for C-TiO_2. Therefore, the study was extended to prepare a number of benzimidazole derivatives using *ortho*-phenylenediamine and various aromatic alcohols in the presence of BHC-TiO_2. Results are summarized in Table 1, in which the high activity of BHC-TiO_2 under visible light irradiation at room temperature was clearly evidenced for a number of benzimidazole derivatives.

The observed unique photocatalytic activity may be attributed to four important features present in BHC-TiO_2 including 1) a high porosity and nanoreactor-like space in the hollow cubic structure, beneficial for the transportation and adsorption of organic substrates; 2) the ultrathin shell, which may facilitate molecular diffusion and create active sites exposed to reactants; 3) the presence of Ti^{3+} species on the surface of BHC-TiO_2 which reduce the band gap of TiO_2 and promote a more efficient electron-hole separation; and 4) the reflecting and scattering of light inside hollow cubic structure which enhances light adsorption by the substrates.

To rule out a potential major contribution of the light intensity of the lamp (500 W visible light vs 15 W UV light experiments) in the superior efficiency of the photocatalysts or the observed high visible light absorption, a model reaction experiment (benzyl alcohol + *o*-phenylenediamine) employing BHC-TiO_2 was conducted with a 60 W UV lamp (4 times higher power). Results provided essentially identical reaction yields (75 vs 73%). These findings pointed out that the light intensity (lamp power) is not the most important factor that leads to efficient photocatalytic behaviour.

Fig. 7a illustrates a plausible light reflecting/scattering mechanism. It is believed that the light inside the hollow cubic structure can be reflected several times, with additional scattering the incident light of different wavelengths in the whole visible light range by the assembled outer shell, these being very appropriate for light harvesting/adsorption by the photocatalyst as well as the organic molecules.

To investigate the effect of the introduction of Ti^{3+} species, an additionally proposed photocatalytic mechanism of BHC-TiO_2 under visible light irradiation is also provided. The introduced Ti^{3+} species can generate sublevel states, which decrease the band gap of TiO_2. As shown in Fig. 7b, the electron is excited to the impurity level in hydrogenated hollow cubic structures upon illumination with visible light. The life of the photo-induced electron in the oxygen vacancy trap is much longer as compared to that on the conductive band, which can desirably reduce oxygen and produce a superoxide radical, improving photocatalytic benzimidazole preparation efficiency. The photo-generated h^+ left in valence band can transfer to alcohol substrates to produce benzyl alcohol cation radicals, and the excited e^- stored in conductive bond can activate the dissolved O_2 to form $\cdot O_2$ radicals. Subsequently, the benzyl alcohol cation radicals can react with $\cdot O_2^-$ radicals to yield the aldehyde intermediate. Subsequently, Lewis acid sites of titania promote a simple reaction between the produced aldehyde and *ortho*-phenylenediamine to afford the corresponding benzimidazoles [46].

3.3. Reusability tests

The recovery and reusability of BHC-TiO_2 was also investigated for the model reaction. In each run, the photocatalyst was recycled and then washed with chloroform and hot ethanol several times. After drying in nitrogen gas flow, BHC-TiO_2 was reused in the synthesis of benzimidazole. Interestingly, this architecture exhibited excelling photocatalytic activities even after seven consecutive runs, with no detectable structure modification or leaching of Ti^{3+} species (33% for reused photocatalyst versus 35% for the fresh nanoarchitecture). This outstanding durability can be attributed to its robust hollow cubic structure against chemical and structural collapse, as verified by XPS, XRD and TEM since all chemical and morphological structures of BHC-TiO_2 were almost fully preserved after 6th reuses (Fig. 8).

4. Conclusions

In summary, we have demonstrated a sequential process for the synthesis of BHC-TiO_2 nanoarchitectures featuring large surface areas $\sim 206\ m^2\ g^{-1}$ and visible light photocatalytic activity. Hydrogenated hollow structure cubes of TiO_2 remarkably improved the visible light photocatalytic activity in benzimidazole preparation compared to typical photocatalysts. In this architecture, the ultrathin porous nanoreactor-like structure is believed to facilitate the transportation and adsorption of organic substrates and the reflecting and scattering of light inside hollow cubic structure enhances light adsorption. Moreover, the presence of Ti^{3+} on the surface reduced the band gap and provided light absorption in the visible region, facilitating electron-hole separation. The proposed strategy led to excellent activities in benzimidazole derivatives preparation. This work can pave the way for the design of different smart architectures of TiO_2 with greatly improved photocatalytic activities and selectivities, probably in alternative photochemical applications such as hydrogen production (water splitting) and solar enhanced fuel cells that will be reported in due course.

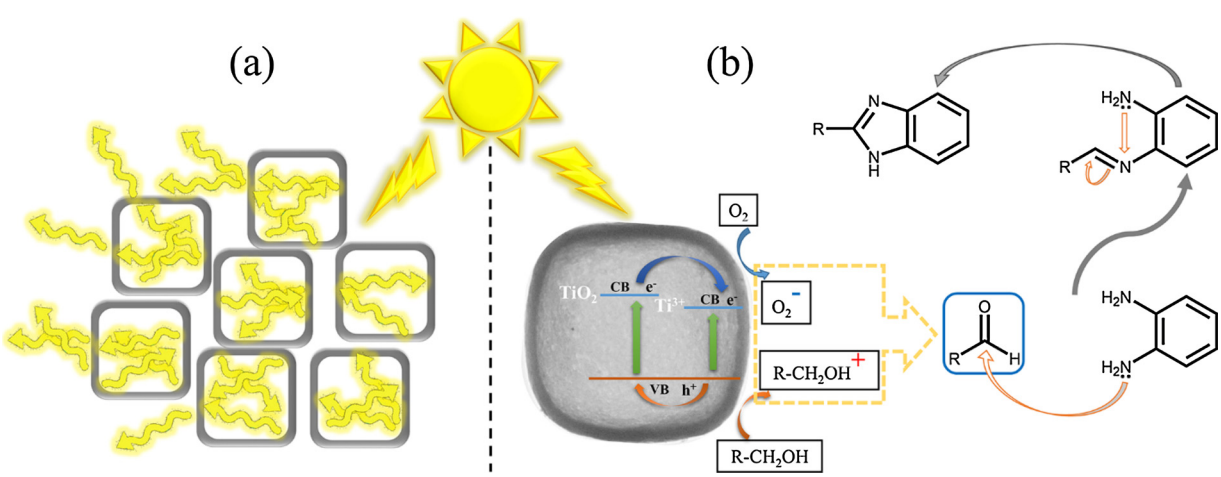

Fig. 7. Schematic diagram of the light scattering effect caused by BHC-TiO_2 nanocubes (a) and schematic of the proposed mechanism for benzimidazole preparation by BHC-TiO_2 architecture.

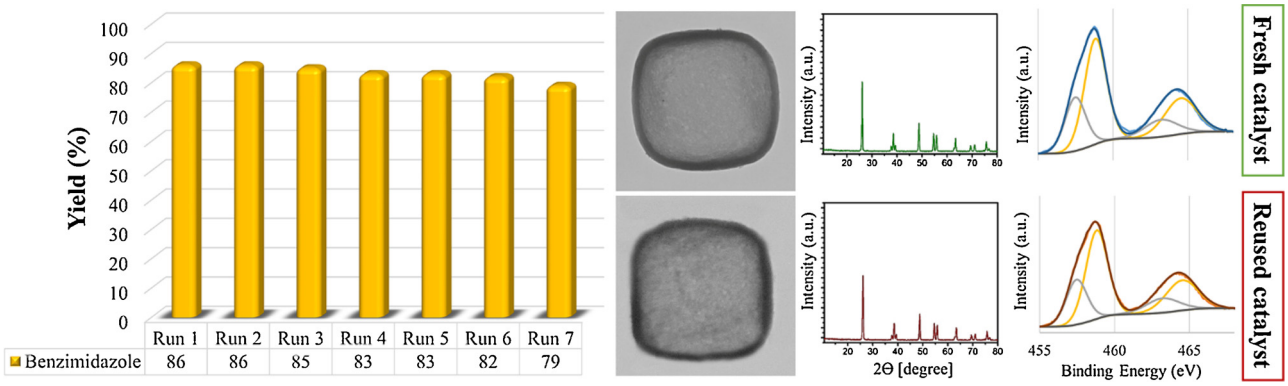

Fig. 8. Reusability study of BHC-TiO_2 in the synthesis of benzimidazole.

Acknowledgements

The authors thank University of Tehran and Universidad de Cordoba for supporting this work. This publication was prepared with support from RUDN University Program 5-100.

Appendix A. Supplementary data

Supplementary material related to this article can be found, in the online version, at doi:https://doi.org/10.1016/j.apcatb.2018.07.020.

References

[1] P. Anastas, N. Eghbali, Chem. Soc. Rev. 39 (2010) 301–312.
[2] D.M. Schultz, T.P. Yoon, Science 343 (2014) 1239176.
[3] D. Friedmann, A. Hakki, H. Kim, W. Choi, D. Bahnemann, Green Chem. 18 (2016) 5391–5411.
[4] S.J. Moniz, S.A. Shevlin, D.J. Martin, Z.-X. Guo, J. Tang, Energy Environ. Sci. 8 (2015) 731–759.
[5] H. Xu, S. Ouyang, L. Liu, P. Reunchan, N. Umezawa, J. Ye, J. Mater. Chem. A 2 (2014) 12642–12661.
[6] J. Schneider, M. Matsuoka, M. Takeuchi, J. Zhang, Y. Horiuchi, M. Anpo, D.W. Bahnemann, Chem. Rev. 114 (2014) 9919–9986.
[7] G. Liu, L. Wang, H.G. Yang, H.-M. Cheng, G.Q.M. Lu, J. Mater. Chem. 20 (2010) 831–843.
[8] G. Liu, H.G. Yang, J. Pan, Y.Q. Yang, G.Q. Lu, H.-M. Cheng, Chem. rev. 114 (2014) 9559–9612.
[9] K. Nakata, A. Fujishima, J. Photochem. Photobiol. 13 (2012) 169–189.
[10] G. Prieto, H. Tüysüz, N. Duyckaerts, J. Knossalla, G.-H. Wang, F. Schüth, Chem. rev. 116 (2016) 14056–14119.
[11] C.C. Nguyen, N.N. Vu, T.-O. Do, J. Mater. Chem. A 3 (2015) 18345–18359.
[12] X. Lai, J.E. Halpert, D. Wang, Energy Environ. Sci. 5 (2012) 5604–5618.
[13] J.B. Joo, Q. Zhang, M. Dahl, I. Lee, J. Goebl, F. Zaera, Y. Yin, Energy Environ. Sci. 5 (2012) 6321–6327.
[14] G. Veerappan, K. Zhang, S. Soman, N. Heo, J.H. Park, Sol. Energy 157 (2017) 434–440.
[15] L. Gao, Y. Li, J. Ren, S. Wang, R. Wang, G. Fu, Y. Hu, Appl. Catal. B: Environ. 202 (2017) 127–133.
[16] J.B. Joo, I. Lee, M. Dahl, G.D. Moon, F. Zaera, Y. Yin, Adv. Funct. Mater. 23 (2013) 4246–4254.
[17] C. Jia, X. Zhang, P. Yang, Appl. Surf. Sci. 430 (2018) 457–465.
[18] R. Kumar, S. Govindarajan, R.K. Siri Kiran Janardhana, T.N. Rao, S.V. Joshi, S. Anandan, ACS appl. mater. Interfaces 8 (2016) 27642–27653.
[19] F. Zuo, K. Bozhilov, R.J. Dillon, L. Wang, P. Smith, X. Zhao, C. Bardeen, P. Feng, Angew. Chem. 124 (2012) 6327–6330.
[20] C. Mao, F. Zuo, Y. Hou, X. Bu, P. Feng, Angew. Chem. Int. Ed. 53 (2014) 10485–10489.
[21] S. Hoang, S.P. Berglund, N.T. Hahn, A.J. Bard, C.B. Mullins, J. Am. Chem. Soc. 134 (2012) 3659–3662.
[22] X. Pan, M.-Q. Yang, X. Fu, N. Zhang, Y.-J. Xu, Nanoscale 5 (2013) 3601–3614.
[23] Q. Zhu, Y. Peng, L. Lin, C.-M. Fan, G.-Q. Gao, R.-X. Wang, A.-W. Xu, J. Mater. Chem. A 2 (2014) 4429–4437.
[24] Y. Yan, M. Han, A. Konkin, T. Koppe, D. Wang, T. Andreu, G. Chen, U. Vetter, J.R. Morante, P. Schaaf, J. Mater. Chem. A 2 (2014) 12708–12716.
[25] Z. Wang, C. Yang, T. Lin, H. Yin, P. Chen, D. Wan, F. Xu, F. Huang, J. Lin, X. Xie, Adv. Funct. Mater. 23 (2013) 5444–5450.
[26] X. Yu, B. Kim, Y.K. Kim, ACS Catal. 3 (2013) 2479–2486.
[27] A. Sinhamahapatra, J.-P. Jeon, J.-S. Yu, Energy Environ. Sci. 8 (2015) 3539–3544.
[28] H. Eskandarloo, M. Hashempour, A. Vicenzo, S. Franz, A. Badiei, M.A. Behnajady, M. Bestetti, Appl. Catal. B: Environ. 185 (2016) 119–132.
[29] A. Ziarati, A. Badiei, R. Luque, W. Ouyang, J. Mater. Chem. A 6 (2018) 8962–8968.
[30] J. Lai, S. Li, F. Wu, M. Saqib, R. Luque, G. Xu, Energy Environ. Sci. 9 (2016) 1210–1214.
[31] S. De, J. Zhang, R. Luque, N. Yan, Energy Environ. Sci. 9 (2016) 3314–3347.
[32] J.C. Colmenares, W. Ouyang, M. Ojeda, E. Kuna, O. Chernyayeva, D. Lisovytskiy, S. De, R. Luque, A.M. Balu, Appl. Catal. B: Environ. 183 (2016) 107–112.
[33] A. Ziarati, A. Badiei, G.M. Ziarani, H. Eskandarloo, Catal. Commun. 95 (2017) 77–82.
[34] T. Sugimoto, Y. Wang, H. Itoh, A. Muramatsu, Colloids Surf. A 134 (1998) 265–279.
[35] W. Li, J. Yang, Z. Wu, J. Wang, B. Li, S. Feng, Y. Deng, F. Zhang, D. Zhao, J. Am. Chem. Soc. 134 (2012) 11864–11867.
[36] Y. Wang, X. Su, S. Lu, J. Mater. Chem. 22 (2012) 1969–1976.
[37] J. Huo, Y. Hu, H. Jiang, C. Li, Nanoscale 6 (2014) 9078–9084.
[38] X. Chen, L. Liu, Y.Y. Peter, S.S. Mao, Science 331 (2011) 746–750.
[39] J. Su, X.-X. Zou, Y.-C. Zou, G.-D. Li, P.-P. Wang, J.-S. Chen, Inorg. chem. 52 (2013) 5924–5930.
[40] X. Jiang, Y. Zhang, J. Jiang, Y. Rong, Y. Wang, Y. Wu, C. Pan, J. Phys. Chem. C 116 (2012) 22619–22624.
[41] G. Wang, H. Wang, Y. Ling, Y. Tang, X. Yang, R.C. Fitzmorris, C. Wang, J.Z. Zhang, Y. Li, Nano lett. 11 (2011) 3026–3033.
[42] J. Chen, Z. Ding, C. Wang, H. Hou, Y. Zhang, C. Wang, G. Zou, X. Ji, ACS appl. mater. Interfaces 8 (2016) 9142–9151.
[43] G. Liu, H.G. Yang, X. Wang, L. Cheng, H. Lu, L. Wang, G.Q. Lu, H.-M. Cheng, J. Phys. Chem. C 113 (2009) 21784–21788.
[44] T. Xia, X. Chen, J. Mater. Chem. A 1 (2013) 2983–2989.
[45] W. Wei, N. Yaru, L. Chunhua, X. Zhongzi, RSC Adv. 2 (2012) 8286–8288.
[46] Y. Shiraishi, Y. Sugano, S. Tanaka, T. Hirai, Angew. Chem. 122 (2010) 1700–1704.